



Published in final edited form as:

*Environ Sci Technol.* 2015 July 07; 49(13): 7784–7792. doi:10.1021/acs.est.5b01026.

## Enhanced Photoreduction of Nitro-aromatic Compounds by Hydrated Electrons Derived from Indole on Natural Montmorillonite

Haoting Tian<sup>†</sup>, Yong Guo<sup>†</sup>, Bo Pan<sup>‡</sup>, Cheng Gu<sup>\*,†</sup>, Hui Li<sup>§</sup>, and Stephen A. Boyd<sup>§</sup>

<sup>†</sup>State Key Laboratory of Pollution Control and Resource Reuse, School of the Environment, Nanjing University, Nanjing 210023, P.R. China

<sup>‡</sup>Faculty of Environmental Science and Engineering, Kunming University of Science and Technology, Kunming 650500, P.R. China

<sup>§</sup>Department of Plant, Soil, and Microbial Sciences, Michigan State University, East Lansing, Michigan 48824, United States

### Abstract

A new photoreduction pathway for nitro-aromatic compounds (NACs) and the underlying degradation mechanism are described. 1,3-Dinitrobenzene was reduced to 3-nitroaniline by the widely distributed aromatic molecule indole; the reaction is facilitated by montmorillonite clay mineral under both simulated and natural sunlight irradiation. The novel chemical reaction is strongly affected by the type of exchangeable cation present on montmorillonite. The photoreduction reaction is initiated by the adsorption of 1,3-dinitrobenzene and indole in clay interlayers. Under light irradiation, the excited indole molecule generates a hydrated electron and the indole radical cation. The structural negative charge of montmorillonite plausibly stabilizes the radical cation hence preventing charge recombination. This promotes the release of reactive hydrated electrons for further reductive reactions. Similar results were observed for the photoreduction of nitrobenzene. In situ irradiation time-resolved electron paramagnetic resonance and Fourier transform infrared spectroscopies provided direct evidence for the generation of hydrated electrons and the indole radical cations, which supported the proposed degradation mechanism. In the photoreduction process, the role of clay mineral is to both enhance the generation of hydrated electrons and to provide a constrained reaction environment in the gallery regions, which increases the probability of contact between NACs and hydrated electrons.

\*Corresponding Author: Phone/Fax: +86-25-89680636. chenggu@nju.edu.cn.

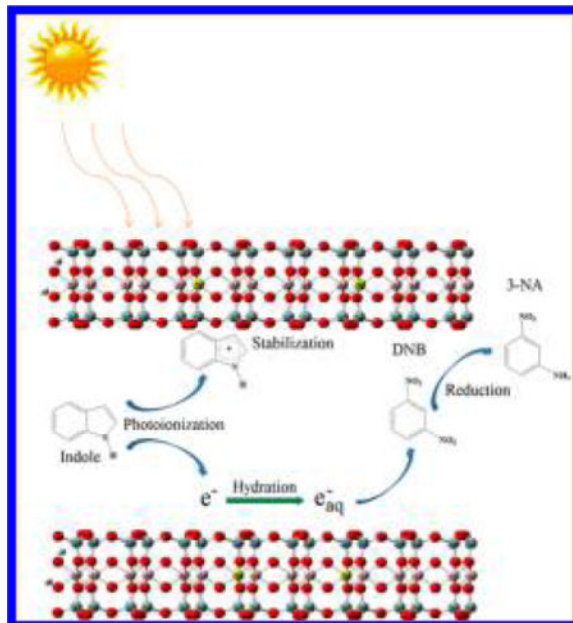
### Supporting Information

Calculated and experimentally observed FTIR frequencies of indole and indole radical cation in the region between 1160 and 1400 cm<sup>-1</sup>; emission spectra of the mercury and xenon lamps used in RTR-EPR and FTIR experiments; degradation of m-DNB in control experiments; degradation of m-DNB by indole in the presence of kaolinite or silica; weather information during sunlight irradiation period; GC-MS chromatogram; degradation of NB under simulated solar light irradiation; the first derivative EPR spectra of indole solution during continuous mercury lamp irradiation; in situ FTIR spectra of indole/Na<sup>+</sup>-montmorillonite, indole/K<sup>+</sup>-montmorillonite, indole/Cs<sup>+</sup>-montmorillonite, and indole only; the optimized molecular structures of indole and indole radical cation as obtained from theoretical calculations; adsorption isotherms of indole and 3-NA on Na<sup>+</sup>-, K<sup>+</sup>-, and Cs<sup>+</sup>-montmorillonite; adsorption isotherms of m-DNB and indole on kaolinite and silica. The Supporting Information is available free of charge on the ACS Publications website at DOI: 10.1021/acs.est.5b01026.

### Notes

The authors declare no competing financial interest.

## Graphical abstract



## INTRODUCTION

Nitro-aromatic compounds (NACs) are widely used as pesticides, explosives, solvents and, chemical intermediates. Prior studies reported that NACs are ubiquitously distributed in the natural environment and have adversely affected human and ecosystem health.<sup>1,2</sup> Reduction of NACs is an important process for complete degradation of NACs in the environment.<sup>3,4</sup> Bacterial and fungi are known to effectively reduce NACs under the proper environmental conditions.<sup>3,5,6</sup> In addition, NACs also undergo abiotic reduction through direct reaction with reduced sulfur, iron species, and extracellular polymeric substances; the reduction reactions were significantly facilitated in the presence of iron porphyrins<sup>7–9</sup> and hydroquinone moieties present in dissolved organic matter, which could serve as electron transfer mediators.<sup>10,11</sup>

Photodegradation is also an important dissipation pathway for NACs.<sup>12</sup> In most cases, hydroxyl radicals were involved in the degradation reaction, which is generally considered as a photooxidation process.<sup>13</sup> However, under some specific environmental conditions, such as in paddy soils, the transformation of NACs is still not fully understood. As rice fields are flooded, the soil becomes anoxic. In addition, due to the shallow depth of water, in such fields photoinduced reactions could also affect the transformation of NACs. Few prior studies have investigated the photodegradation process for some chloroaromatic and nitro-group containing pesticides, e.g. carfentrazone-chloropropionic acid<sup>14</sup> and nitrofen<sup>15</sup> in sunlit rice paddies. Further research is needed to elucidate other possible photodegradation pathways for organic contaminants, especially NACs under anaerobic conditions.

As the most active reducing species, the hydrated electron is localized and stabilized within a cavity formed by surrounding water molecules, which could be generated by ultraviolet

light irradiation of aromatic compounds such as indole in aqueous solution.<sup>16–21</sup> When aromatics are excited to their first singlet state by light irradiation, aromatic radical cations and hydrated electrons are produced after charge separation.<sup>22</sup> Previous studies showed that hydrated electrons could reduce many organic and inorganic contaminants,<sup>23,24</sup> as well as perfluorinated compounds.<sup>25,26</sup> However, due to the strong reductive ability, the lifetime of hydrated electrons in solution is short, as it is quickly consumed by surrounding protons and oxygen or quenched through charge recombination.<sup>27,28</sup> As a result, there are few documented instances for the degradation of contaminants by hydrated electrons under environmentally relevant conditions.

Smectites, including montmorillonite, are 2:1 layered aluminosilicate clay minerals that are widely distributed in soils, subsoils, sediments, and prehistoric clay deposits.<sup>29</sup> Due to isomorphic substitution in the tetrahedral Si and/or octahedral Al layers, smectites possess structural negative charges that are compensated by exchangeable cations. With their exceptionally large surface areas, smectites can function as efficient adsorbents for many organic compounds, including NACs, and the adsorption of NACs is strongly dependent on the exchangeable cations.<sup>30,31</sup> More interestingly, the unique structure of smectite clays could induce the formation of organic radical cations<sup>32,33</sup> and subsequently localize these radicals in the interlayer regions.<sup>29,34–36</sup> Related studies have shown that the smectite clay could effectively stabilize the photoinduced charge separation state thereby prolonging its lifetime from a few milliseconds to several hours.<sup>37</sup> Here, we hypothesize that the presence of natural smectite clay minerals enhances the production of hydrated electrons by facilitating the separation of electrons and radical cations during the light irradiation of certain aromatic structures and the formed hydrated electrons could effectively reduce NACs adsorbed on clay surfaces.

The objective of this study was to investigate the mechanism for production of photoinduced hydrated electrons and subsequent reduction of NACs facilitated by natural montmorillonite clay. In this research, 1,3-dinitrobenzene (m-DNB) and indole were used as a model NAC and as a representative aromatic compound capable of generating hydrated electrons, respectively. Previous studies have shown that m-DNB was strongly adsorbed onto montmorillonite surfaces.<sup>30,31</sup> In addition, indole and its derivatives (e.g., indole-3-acetic acid) are considered as common components of natural soil or sediment organic matter<sup>38–40</sup> and have been widely detected in the environment. Our experimental results showed that m-DNB can be reduced to 3-nitroaniline (3-NA) by hydrated electrons derived from indole in the presence of montmorillonite clay when irradiated by either simulated or natural sunlight. The reductive process is strongly affected by the exchangeable cations in clay interlayer, following the order: Cs<sup>+</sup> saturated montmorillonite (Cs<sup>+</sup>-montmorillonite) > K<sup>+</sup> saturated montmorillonite (K<sup>+</sup>-montmorillonite) > Na<sup>+</sup> saturated montmorillonite (Na<sup>+</sup>-montmorillonite). The key role of montmorillonite, in addition to promoting the production of hydrated electrons, is to provide a unique matrix that increases direct contact between hydrated electrons and NACs.

## ■ MATERIALS AND METHODS

### Chemicals

Analytical grade nitrobenzene (NB), m-DNB, aniline, 3-NA, indole, 5,5-dimethyl-1-pyrroline *N*-oxide (DMPO), sodium acetate, NaCl, KCl, and CsCl were all obtained from Sigma-Aldrich with purity >98%. Sodium dihydrogen phosphate (>99%, NaH<sub>2</sub>PO<sub>4</sub>) and sodium phosphate dibasic (>99%, Na<sub>2</sub>HPO<sub>4</sub>) were purchased from Shanghai Chemical Reagent CO. (Shanghai, China). Acetonitrile was of HPLC grade from Tedia Inc. (Fairfield, OH). All the chemicals were used as received.

### Preparation of Homoionic Na<sup>+</sup>-, K<sup>+</sup>-, and Cs<sup>+</sup>-Montmorillonite

Montmorillonite was obtained from Fenghong Inc. (Zhejiang Province, China). Cation exchange capacity (CEC) of the montmorillonite was measured as 770 mmol kg<sup>-1</sup>. The preparation of Na<sup>+</sup>, K<sup>+</sup>, and Cs<sup>+</sup> saturated montmorillonite followed the method described by Arroyo et al.<sup>41</sup> Briefly, the clay suspension was first titrated to pH 6.8 with 0.5 M sodium acetate buffer (pH = 5) to remove carbonate impurities. Clay-sized particles (<2 μm) were obtained by centrifugation of the clay suspension for 6 min at 60 g, and the clay fraction was resuspended in 0.1 M NaCl, KCl or CsCl solution for 8 h, then centrifuged at 3295 g for 20 min, and the supernatant was discarded. This procedure was repeated six times to ensure montmorillonite cation exchange sites were fully saturated by Na<sup>+</sup>, K<sup>+</sup>, or Cs<sup>+</sup>. The Na<sup>+</sup>-, K<sup>+</sup>-, or Cs<sup>+</sup>-montmorillonite was then washed using Milli-Q water until free of chloride as indicated by a negative test with AgNO<sub>3</sub> and, then, freeze-dried to receive clay powders. Silica and kaolinite (>99%) were used as controls and purchased from Nanjing Chemical Reagent CO. (Nanjing, China) and Sigma-Aldrich, respectively, with purity >99%.

### Batch Adsorption Experiments

The adsorption of indole, m-DNB and 3-NA on Na<sup>+</sup>-, K<sup>+</sup>-, Cs<sup>+</sup>-montmorillonite was conducted by a standard batch equilibrium method. For each experiment, Na<sup>+</sup>-, K<sup>+</sup>-, or Cs<sup>+</sup>-montmorillonite clay (10 mg) was weighed into a 15 mL glass centrifuge tube containing 10.0 mL solution of adsorbate, with the initial concentrations ranging from 0.005 to 0.2 mM for m-DNB, 3-NA, and from 0.05 to 1.25 mM for indole. A constant pH of 7.3 was maintained using 5 mM phosphate buffer. The centrifuge tubes were covered with aluminum foil to prevent exposure to light and shaken at 40 rpm on a rotary shaker for 24 h at room temperature (~25 °C), and then centrifuged at 1250 g for 20 min. Preliminary studies showed that adsorption equilibrium was achieved within this time period. There was no significant loss of adsorbate due to adsorption to glassware or other transformation under our experimental conditions. The concentration of indole, m-DNB, or 3-NA in supernatant was analyzed by high performance liquid chromatography (HPLC) (Waters Alliance 2695, Milford, MA) monitored at 262 nm for indole and m-DNB and 227 nm for 3-NA using a Waters 2998 photodiode array detector. A 4.6 mm × 250 mm Waters XBridge Shield C18 column was used, and the mobile phase was a mixture of acetonitrile/water at 35:65 with a flowrate of 1 mL min<sup>-1</sup>. The amount of adsorbate adsorbed on montmorillonite was calculated from the difference between the concentrations of blanks (no clay) and the supernatants from the sorbent-containing samples. The adsorption of m-DNB and indole on kaolinite and silica was also conducted under the same reaction conditions.

### Photoreduction of m-DNB by Indole on Montmorillonite Mineral Surfaces

The photoreduction experiments were conducted in a simulated soil colloid solution (10 mL) containing montmorillonite clay (or silica and kaolinite) ( $1 \text{ g L}^{-1}$ ), indole (0.5 mM), m-DNB (0.0125 mM), and phosphate buffer (5 mM, pH = 7.3) using a XPA-7 model photochemical reactor (Xujiang Electromechanical Inc., Nanjing, China). A 500W xenon lamp (Institute of Electric Light Source, Beijing) was used to simulate solar light irradiation, which was positioned in the cylindrical quartz cold trap. The light intensity on the surface of the reaction tube was  $45 \text{ mW cm}^{-2}$  as recorded by a radiometer (CEL-NP2000-10, Ceaulight, Beijing, China). Before the photoreaction, all water used in the experiment was fully deoxygenated by purging with  $\text{N}_2$  for 1 h. The quartz reaction tubes were then placed within the merry-go-round at the center of the reactor and rotated at 8 rpm to ensure uniform exposure. A magnetic stir bar was placed in each tube to provide stirring. The temperature of the reaction was maintained at  $25^\circ\text{C}$  by a constant temperature water bath. At predetermined time interval over the course of reaction, samples were sacrificed and transferred to a centrifuge tube. The reaction products were extracted by adding 10 mL acetonitrile for 8 h, then the tube was centrifuged at  $1250 \text{ g}$  for 20 min. Preliminary experiments indicated that the recoveries for m-DNB and its major reduction product 3-NA were  $>95\%$ , respectively. The concentrations of m-DNB and the reaction products in supernatant were analyzed by the same HPLC system as mentioned above. To further investigate other possible degradation pathways, the reaction products were also analyzed by a Thermo gas chromatograph fitted with a mass spectrometer (GC-MS, Trace ISQ) on full scan mode (50 to  $800 \text{ amu}$ ) after the sample was extracted with 10 mL *n*-hexane for 8 h and concentrated to 1 mL. A HP-5 MS capillary column (length = 30 m; internal diameter =  $250 \mu\text{m}$ ; film thickness =  $0.25 \mu\text{m}$ ) was employed. Helium was the carrier gas at a flow rate of  $1 \text{ mL min}^{-1}$  with splitless injection at  $280^\circ\text{C}$ . The oven temperature was programmed from  $60^\circ\text{C}$  (2 min hold) to  $150^\circ\text{C}$  ( $10^\circ\text{C min}^{-1}$ , 5 min hold), and then to  $280^\circ\text{C}$  ( $15^\circ\text{C min}^{-1}$ , 2 min hold). Dark control experiments were also carried out by wrapping the tubes with aluminum foil and shaken at 40 rpm on a rotary shaker. All the experiments were conducted in triplicate. The photodegradation of NB under the same reaction conditions was also investigated.

Similar experiments were carried out under natural sunlight irradiation. Samples were exposed to sunlight from 9 a.m. to 5 p.m. on sunny or partially cloudy days from March 22, 2014, to March 27, 2014, on the roof of the environmental science and engineering building of Kunming University of Science and Technology (Kunming, Yunnan province,  $102^\circ51' \text{ E}$ ,  $24^\circ50' \text{ N}$ , altitude: 1954 m). Reaction vessels were quartz tubes ( $16 \text{ mm} \times 150 \text{ mm}$ ) and were fixed on a rotary shaker by end-over-end rotation at 15 rpm. The rotator was positioned toward the sun once every hour. When not exposed to sunlight, samples were kept in the dark. During the irradiation period, the information on solar intensity, humidity, and temperature at the experimental site was recorded with a radiometer (UV-B, FZ-A, photoelectric instrument factory of Beijing Normal University, Beijing, China) and a hygrothermograph (DT8002, Kejian, Shanghai, China). At specific time interval, samples were sacrificed and analyzed by HPLC and GC-MS.

## In Situ Electron Paramagnetic Resonance and Fourier Transform Infrared Measurements

In situ irradiation time-resolved electron paramagnetic resonance (RTR-EPR) was conducted on a Bruker X-band A300-6/1 EPR spectrometer at room temperature. DMPO was used as the effective ion trap to scavenge the generated hydrated electrons in the reaction. The initial concentrations of indole, DMPO, and montmorillonite clay were 0.5 mM, 10 mM, and 1 g L<sup>-1</sup>, respectively. For each RTR-EPR measurement, 20  $\mu$ L reaction mixture was filled into a quartz thin-wall EPR tube (707-SQ-250M, Wilmad, USA). The parameters used for EPR measurement were the following: microwave frequency of 9.87 GHz, modulation frequency of 100 kHz, microwave power of 20 mW, modulation amplitude of 1 G, receiver gain of  $1.0 \times 10^3$ , sweep width of 100 G, center field of 3518 G. The relative intensity of radical response was measured as peak-to-peak height. The irradiation system was provided by an arc light source (LOT-Oriel GmbH & Co. KG, Germany), equipped with a 100 W mercury lamp (USH-102D, Ushio, Japan). The emission spectrum of the mercury lamp is shown in Figure S1a. The light can go through the window-shades of the resonant cavity onto the sample for in situ irradiation.

Fourier transform infrared (FTIR) spectra were collected using a Bruker tensor 27 FTIR spectrometer equipped with a mercury cadmium telluride detector and an attenuated total reflection (ATR) flow cell accessory (Pike Technology, USA). A total of 64 scans with a spectral resolution of 2 cm<sup>-1</sup> were employed. To increase the aqueous solubility, indole was dissolved in methanol/phosphate buffer mixture, in which the methanol fraction was kept at 5%. The sample was prepared by initially mixing 100 mg clay with 10 mL indole solution (10 mM) on a rotary shaker at 40 rpm for 3 h. Then the clay suspension was centrifuged, after the supernatant was discarded, the clay paste was collected and uniformly applied to the ATR element. Nitrogen atmosphere was maintained during sample preparation and FTIR measurement. The IR spectra of indole solution (10 mM) and clay paste without indole were also collected. The spectrum attributable only to indole in indole/clay mixture was obtained by subtraction of the clay/phosphate buffer paste signal from the indole/clay paste spectrum. A 500 W xenon lamp (CEL-S500, Ceaulight, Beijing, China) was used as the light source for in situ FTIR measurement, and the lamp was fixed on the top of the ATR cell with a distance of 25 cm. The emission spectrum of the xenon lamp is shown in Figure S1b

## Computational Methods

B3LYP methods<sup>42</sup> in Gaussian 03 program<sup>43</sup> have been performed to investigate the structure and infrared spectra of indole and indole radical cation. Full atom model was adopted for indole and indole radical cation. The 6-311++(d,p) basis set was applied to C, H, and N atoms. All molecular structures were constructed with Gview program based on the optimized results.

## ■ RESULTS AND DISCUSSION

### Photoreduction of m-DNB Catalyzed by Natural Montmorillonite

As shown in Figure S2, in dark (no irradiation) control experiments, there is no degradation of m-DNB in any samples (Figure S2a). In addition, even under light irradiation, negligible degradation (>95% recovery) of m-DNB was observed in the absence of indole under anoxic

condition (Figure S2b). When indole was added, a significant portion of m-DNB is reduced to 3-NA (Figure 1a, b, c, d). No further reduction to m-phenylenediamine was observed. These results clearly showed that natural montmorillonite clay mineral greatly enhanced the transformation process, i.e. the reduction of m-DNB. The fraction of m-DNB converted to 3-NA increased from 4.9% (indole only) to 11.1, 19.8, and 31% in the presence of Na<sup>+</sup>, K<sup>+</sup>, and Cs<sup>+</sup> saturated montmorillonite after 24 h reaction period, respectively (Figure 1a, b, c, d). The reduction of m-DNB is attributed to production of hydrated electrons induced by light irradiation of indole, which subsequently reduced m-DNB to 3-NA. Furthermore, this process was facilitated by the unique structure of montmorillonite clay mineral. For comparison, when silica and kaolinite were used to represent the nonexpandable minerals, only slight increases for reduction of m-DNB (6.8 and 6.5% in the presence of kaolinite and silica) were observed (Figure S3), which indicates that the photoreduction process mainly occurs in the interlayer region of montmorillonite. Similar results were also found in sunlight irradiation experiments. Natural sunlight induced the reduction of m-DNB to 3-NA by indole, and the formation of 3-NA as a function of exchangeable cation followed the same order: Cs<sup>+</sup>-montmorillonite (14.6%) > K<sup>+</sup>-montmorillonite (11.4%) > Na<sup>+</sup>-montmorillonite (7.3%) > indole only (1.4%) (Figure 2). Solar intensity, humidity and temperature for the days when sunlight experiments were conducted is listed in Figure S4. A good mass balance (>90%) was obtained for simulated sunlight experiments during the reaction period (24 h) (Figure 1), indicating that reduction to 3-NA is the predominant process. Under natural sunlight, with much longer reaction time, the mass balance was initially over 90% in the first 4 d; as the reaction proceeds the recovery (m-DNB + 3-NA) decreased to 86% for Cs<sup>+</sup>-montmorillonite system after 6 d (Figure 2d). This could plausibly be explained by the leakage of atmospheric O<sub>2</sub> into the system. As suggested in the literature, hydrated electrons could react with O<sub>2</sub> to form superoxide radical (O<sub>2</sub><sup>•-</sup>) and H<sub>2</sub>O<sub>2</sub>,<sup>28</sup> and these reactive species might react further with organic contaminants, which is indicated by our GC-MS analysis. For the system with Cs<sup>+</sup>-montmorillonite, after 6 d reaction some oxidation products from m-DNB and indole were observed. Isatin (product A) (Figure S5b) and formanilide (product D) (Figure S5e) result from the oxidation and ring cleavage of indole molecules.<sup>44</sup> Phenyl phenylacetate (product B) (Figure S5c) results from the condensation of phenol and phenylacetic acid, which are the common oxidation products from m-DNB and indole, respectively,<sup>45</sup> by direct esterification. Due to the complexity of the oxidation reactions, other reaction products in GC-MS chromatogram were not fully identified (Figure S5a).

To extend our results to another NAC, NB was also used. Similarly, under simulated sunlight condition we observed that the reduction of NB to aniline was promoted by the presence of Na<sup>+</sup>-montmorillonite; the production of aniline after 24 h was 7.7% compared to 1.6% in the absence of the clay mineral (Figure S6).

### In Situ RTR-EPR and FTIR Analysis

To further investigate the underlying reaction mechanism, in situ RTR-EPR and FTIR spectroscopic techniques were utilized to monitor the photo-induced reduction reaction of m-DNB. The protonated DMPO-electron spin adduct (DMPO-H) was detected during continuous irradiation of samples containing indole and 10 mM DMPO with and without

clay minerals (Figure S7). The spin Hamiltonian parameters observed for DMPO-H spin adduct are in good agreement with literature values.<sup>46</sup> Nine peaks with the intensity ratio of 1:1:2:1:2:1:2:1:1 were observed, and the EPR parameters are  $a(\text{N},\text{NO}) = 16.51 \pm 0.01$  G,  $a(\text{H},\text{CH}_2) = 22.59 \pm 0.01$  G, respectively, indicating the formation of hydrated electrons after irradiation of indole molecules. The time-dependent changes of the EPR signals are shown in Figure 3. The DMPO-H signals increased quickly during the irradiation period and decreased gradually once irradiation was stopped. The presence of montmorillonite, especially  $\text{Cs}^+$ -montmorillonite, significantly enhanced the production of photoinduced hydrated electrons, which explains the higher photoreduction of m-DNB in the presence of the natural clay mineral (Figure 3).

Due to the strong IR absorption below frequencies of  $1160\text{ cm}^{-1}$  by the clay structure and the strong interference around  $1600\text{ cm}^{-1}$  from  $\text{H}_2\text{O}$ , only the IR bands attributed to indole in the region between  $1160$  and  $1400\text{ cm}^{-1}$  were distinctly identified. In accordance with IR band assignments reported in the literature,<sup>47,48</sup> peaks for indole are as follows (Table S1): vibrations of the pyrrole ring in-plane stretching and N-H bending ( $1207\text{ cm}^{-1}$ ), synchronous bending of hydrogen in both rings ( $1248\text{ cm}^{-1}$ ), pyrrole ring in-plane bending and stretching ( $1280\text{ cm}^{-1}$ ), benzene ring in-plane stretching and C-N stretching ( $1338\text{ cm}^{-1}$ ), and asynchronous bending of hydrogen in both rings ( $1354\text{ cm}^{-1}$ ) (lines 1, 2, 3, 4, and 5 in Figure 4c). Upon irradiation, a new peak at  $1200\text{ cm}^{-1}$  (line 3' in Figure 4) appeared in the indole/clay system (Figure 4e, f, g). Furthermore, the  $1200\text{ cm}^{-1}$  peak only appeared during the irradiation and disappeared quickly in the absence of light (Figure S8, S9, and S10). In contrast, for indole only system, no such peak was observed (Figure 4d and S11). We attribute the new light-induced peak at  $1200\text{ cm}^{-1}$  to the indole radical cation. Similar results were reported in our previous study of radical cation formation from pentachlorophenol on  $\text{Fe}^{3+}$  saturated montmorillonite, and it is involved in the formation of octachlorodibenzodioxin.<sup>36</sup>

To better understand the IR spectral peak shifts that occurred upon irradiation of the clay/indole suspension, theoretical spectra of the indole and indole radical cation were calculated and compared with our experimental results (Figure 4a–c). The optimized geometries of indole and indole radical cation molecules in gas phase are shown in Figure S12. The computed spectrum of indole agrees well with the experimental results (Figure 4a and c and Table S1). Compared to indole molecule, the calculated vibrational peaks in the region of  $1160$ – $1400\text{ cm}^{-1}$  for indole radical cation have red shifts to lower frequencies as the loss of an electron might weaken the C–C/C–N bonds within the pyrrole and benzene rings, and part of C–H bonds (Figure S12 and Table S1). According to peak intensity ratios and the vibrational pattern, the two predominant IR peaks at  $1185$  and  $1235\text{ cm}^{-1}$  in the spectrum of indole radical cation correspond to  $1287$  and  $1263\text{ cm}^{-1}$  peaks in molecular (neutral) indole, respectively. The more significant IR shift for the pyrrole ring bending and stretching peak ( $-102\text{ cm}^{-1}$ , from  $1287$  to  $1185\text{ cm}^{-1}$ ) can plausibly be attributed to the stronger disturbance on the pyrrole ring caused by the extraction of one electron from indole. For the peak corresponding to the synchronous bending of hydrogen ( $-28\text{ cm}^{-1}$ , from  $1263$  to  $1235\text{ cm}^{-1}$ ), changes in the lengths of C–H bonds are limited (Figure S12). Due to the low yield of indole radical cations in the system, only the peak with the highest intensity ( $1200\text{ cm}^{-1}$ ) was observed in our experiment, which is also in good agreement with the calculated value

(1185  $\text{cm}^{-1}$ ) by first principle density functional theory (DFT). The slight discrepancy between computational results and the experimental spectra can be attributed to the complexity of indole/clay system, since in the theoretical calculations we only considered the indole and indole radical cation molecules in an isolated ideal condition, whereas in the actual experimental sample, the clay structure likely influences the IR band positions.<sup>36</sup> Our experimental (FTIR) and theoretical (DFT) results mutually support the formation of indole radical cation in the experimental system containing clay and suggest that the radical cation produced after charge separation could be stabilized by the planar negatively charged clay surface.

### Effects of Exchangeable Cations on Photoreduction of m-DNB

Another interesting observation in our photo-reduction reaction is that the degradation process is strongly affected by the type of exchangeable cations in clay interlayer (Figures 1 and 2). The magnitude and rate for reduction of m-DNB is the highest on  $\text{Cs}^+$ -montmorillonite, followed by  $\text{K}^+$ -montmorillonite and then  $\text{Na}^+$ -montmorillonite. It has been well documented that  $\text{Cs}^+$ , with the lowest hydration energy and smallest hydration sphere ( $-258 \text{ kJ mol}^{-1}$  and  $3.6 \text{ \AA}$ ) compared to  $\text{K}^+$  ( $-304 \text{ kJ mol}^{-1}$  and  $5.3 \text{ \AA}$ ) and  $\text{Na}^+$  ( $-375 \text{ kJ mol}^{-1}$  and  $7.9 \text{ \AA}$ ), manifests more unobscured clay siloxane domains for adsorption and these surfaces are relatively less hydrated.<sup>49–51</sup> Furthermore, complexes between exchangeable cations and the nitro groups of NACs are more energetically favorable for the weakly hydrated cations, which promotes the adsorption of NACs by  $\text{Cs}^+$ -montmorillonite clay.<sup>51</sup> The adsorption of m-DNB on montmorillonite with different exchangeable cations also shows much higher adsorption of m-DNB on  $\text{Cs}^+$ -montmorillonite compared to  $\text{Na}^+$ - or  $\text{K}^+$ -clay (Figure 5). The adsorption coefficient ( $K_d = 2121.12 \text{ L kg}^{-1}$ ) on  $\text{Cs}^+$ -montmorillonite is 179 and 1727 times higher than those on  $\text{K}^+$ -montmorillonite ( $K_d = 11.82 \text{ L kg}^{-1}$ ) and  $\text{Na}^+$ -montmorillonite ( $K_d = 1.23 \text{ L kg}^{-1}$ ), respectively (Table 1). Indole could also be adsorbed onto montmorillonite surfaces (Figure S13), and the fitted adsorption coefficients follow the same order of  $\text{Cs}^+$ -montmorillonite ( $5.13 \text{ L kg}^{-1}$ )  $>$   $\text{K}^+$ -montmorillonite ( $3.88 \text{ L kg}^{-1}$ )  $\approx$   $\text{Na}^+$ -montmorillonite ( $3.92 \text{ L kg}^{-1}$ ) (Table 1). Hence, the adsorption results clearly indicate that montmorillonite with less hydrated cations could more effectively concentrate both m-DNB and indole in the constrained interlayer region of the clay mineral thereby increasing the contact possibilities between m-DNB and hydrated electrons. This would explain the cation-dependence for the photoreduction process observed in our experiments.

### Proposed Mechanism for Photoreduction of NACs Catalyzed by Natural Montmorillonite

Based on our experimental and spectroscopic results, the mechanism for photoreduction of NACs by indole in the presence of natural montmorillonite can be described as follows: Indole and NAC molecules are initially adsorbed in the gallery regions or interlayers of montmorillonite. Upon light irradiation, photolysis of indole molecules associated with the clay mineral produces hydrated electrons and the indole radical cations. Due to the planar layered aluminosilicate structure with embedded negative charges, montmorillonite clay could stabilize the newly formed radical cations, consequently preventing the recombination of hydrated electrons and indole radical cations, which would increase the concentration of hydrated electrons. Finally, NACs adsorbed on clay surface are reduced to corresponding

anilines by the hydrated electrons. For minerals without interlayer region (e.g., silica and kaolinite), only limited adsorption (Figures S14 and 15 and Table 1) and insignificant increase for reduction of NACs (Figure S3) were observed, which can be attributed to the lower surface area and the lack of negatively charged surface. During the photoreduction process, the role of montmorillonite clay mineral is not only to promote the separation of electron and organic cation, but also it acts as a nanoreactor in which both NACs and hydrated electrons accumulate in a constrained environment, hence promoting their direct contact. Therefore, a higher photoreduction rate is expected for pollutants with greater adsorption, i.e. strong adsorption of NACs in the clay interlayers is a prerequisite for effective photoreduction in the montmorillonite-indole system. It could also partially explain why no further reduction of 3-nitroaniline to m-phenylenediamine occurs. As shown in Figure S16 and Table 1, there is negligible adsorption for 3-nitroaniline on montmorillonite. After 3-nitroaniline is produced, it may be released from clay surface into aqueous solution, thereby decreasing the possibility for further contact with hydrated electrons.

### Environmental Implications

Our results demonstrate that NACs can be photoreduced in the presence of indole and the clay mineral montmorillonite under neutral pH and simulated irradiation conditions. Natural sunlight exposure experiments further support that the photoreduction process could occur naturally, which is a previously unknown route for the degradation of NACs in natural environment. It has been well established that many persistent organic contaminants, e.g. polychlorinated biphenyls and polychlorinated dibenzo-dioxins, could form strong interaction with montmorillonite and be intercalated in a clay interlayer.<sup>29,35,36</sup> Furthermore, indoles are common organic molecules found in the environment. The primary natural source of indoles is from feces of animals, microbial decomposition of proteins, and secretion of various plants and microbes.<sup>52–56</sup> The concentration of indoles has been reported to be in the part per million ( $\text{mg L}^{-1}$ ) level in natural environments,<sup>52,53,56</sup> and in the dozens of  $\text{mg L}^{-1}$  in coking and swine wastewater.<sup>57,58</sup> Therefore, it is reasonable that other contaminants could undergo a similar degradation reaction. The new photoreduction pathway described herein improves our understanding for the transformation of persistent organic pollutants in the natural environment.

### Supplementary Material

Refer to Web version on PubMed Central for supplementary material.

### Acknowledgments

This work was financially supported by the National Science Foundation of China (grants 21222704), National Key Basic Research Program of China (2014CB441102), the Collaborative Innovation Center for Regional Environmental Quality and Grant P42 ES004911 from the National Institute of Environmental Health Sciences (NIEHS), National Institutes of Health (NIH), and by the Michigan AgBioResearch. The contents are solely the responsibility of the authors and do not necessarily represent the official views of NIEHS or NIH. We thank the Analytical Center and High Performance Computing Center of Nanjing University for the characterization of samples and computational study.

## References

1. Kang FX, Zhu DQ. Abiotic Reduction of 1, 3-Dinitrobenzene by Aqueous Dissolved Extracellular Polymeric Substances Produced by Microorganisms. *J Environ Qual*. 2012; 42(5):1441–1448.
2. Fu HY, Zhu DQ. Graphene oxide-facilitated reduction of nitrobenzene in sulfide-containing aqueous solutions. *Environ Sci Technol*. 2013; 47(9):4204–4210. [PubMed: 23561007]
3. Spain JC. Biodegradation of nitroaromatic compounds. *Annu Rev Microbiol*. 1995; 49:523–555. [PubMed: 8561470]
4. Gu C, Jia HZ, Li H, Teppen BJ, Boyd SA. Synthesis of highly reactive subnano-sized zero-valent iron using smectite clay templates. *Environ Sci Technol*. 2010; 44(11):4258–4263. [PubMed: 20446730]
5. Alexander M, Lustigman BK. Effect of chemical structure on microbial degradation of substituted benzenes. *J Agric Food Chem*. 1966; 14(4):410–413.
6. Kulkarni M, Chaudhari A. Microbial remediation of nitroaromatic compounds: an overview. *J Environ Manage*. 2007; 85(2):496–512. [PubMed: 17703873]
7. Heijman CG, Holliger C, Glaus MA, Schwarzenbach RP, Zeyer J. Abiotic reduction of 4-chloronitrobenzene to 4-chloroaniline in a dissimilatory iron-reducing enrichment culture. *Appl Environ Microbiol*. 1993; 59(12):4350–4353. [PubMed: 16349133]
8. Klausen J, Troeber SP, Haderlein SB, Schwarzenbach RP. Reduction of substituted nitrobenzenes by Fe (II) in aqueous mineral suspensions. *Environ Sci Technol*. 1995; 29(9):2396–2404. [PubMed: 22280284]
9. Hofstetter TB, Heijman CG, Haderlein SB, Holliger C, Schwarzenbach RP. Complete reduction of TNT and other (poly) nitroaromatic compounds under iron-reducing subsurface conditions. *Environ Sci Technol*. 1999; 33(9):1479–1487.
10. Schwarzenbach RP, Stierli R, Lanz K, Zeyer J. Quinone and iron porphyrin mediated reduction of nitroaromatic compounds in homogeneous aqueous solution. *Environ Sci Technol*. 1990; 24(10):1566–1574.
11. Dunnivant FM, Schwarzenbach RP, Macalady DL. Reduction of substituted nitrobenzenes in aqueous solutions containing natural organic matter. *Environ Sci Technol*. 1992; 26(11):2133–2141.
12. Wang AM, Hu C, Qu JH, Yang M, Liu HJ, Ru J, Qi R, Sun JF. Phototransformation of nitrobenzene in the Songhua river: kinetics and photoproduct analysis. *J Environ Sci*. 2008; 20(7):787–795.
13. Vione D, Falletti G, Maurino V, Minero C, Pelizzetti E, Malandrino M, Ajassa R, Olario RI, Arsene C. Sources and sinks of hydroxyl radicals upon irradiation of nature water samples. *Environ Sci Technol*. 2006; 40(12):3775–3781. [PubMed: 16830541]
14. Ngim KK, Crosby DG. Photoreduction of the chloropropionic acid of carfentrazone-thyl in sodium sulfide crane flat meadow solutions. *Environ Toxicol Chem*. 2002; 20(10):2007–2013.
15. Nakagawa M, Crosby DG. Photodecomposition of Nitrofen. *J Agric Food Chem*. 1974; 22(5):849–853. [PubMed: 4422724]
16. Hart EJ, Boag JW. Absorption spectrum of the hydrated electron in water and in aqueous solutions. *J Am Chem Soc*. 1962; 84(21):4090–4095.
17. Joschek H-I, Grossweiner LI. Optical Generation of Hydrated Electrons from Aromatic Compounds. II<sup>1</sup>. *J Am Chem Soc*. 1966; 88(14):3261–3268. [PubMed: 5946592]
18. Swallow AJ. Hydrated electrons in seawater. *Nature*. 1969; 222:369–370.
19. Bragg AE, Verlet JRR, Kammrath A, Cheshnovsky O, Neumark DM. Hydrated electron dynamics: From clusters to bulk. *Science*. 2004; 306(5696):669–671. [PubMed: 15375222]
20. Verlet JRR, Bragg AE, Kammrath A, Cheshnovsky O, Neumark DM. Observation of large water-cluster anions with surface-bound excess electrons. *Science*. 2005; 307(5706):93–96. [PubMed: 15604360]
21. Neumark DM. Ultrafast spectroscopy: Ejecting electrons from water. *Nat Chem*. 2010; 2(4):247–248. [PubMed: 21124498]

22. Feitelson J, Hayon E. Electron ejection and electron capture by phenolic compounds. *J Phys Chem.* 1973; 77(1):10–15.
23. Li XC, Fang JY, Liu GF, Zhang SJ, Pan BC, Ma Jun. Kinetics and efficiency of the hydrated electron-induced dehalogenation by the sulfite/UV process. *Water Res.* 2014; 62:220–228. [PubMed: 24956604]
24. Chaychian M, Al-Sheikhly M, Silverman J, McLaughlin WL. The mechanisms of removal of heavy metals from water by ionizing radiation. *Radiat Phys Chem.* 1998; 53(2):145–150.
25. Qu Y, Zhang CJ, Li F, Chen J, Zhou Q. Photo-reductive defluorination of perfluorooctanoic acid in water. *Water Res.* 2010; 44(9):2939–2947. [PubMed: 20227745]
26. Song Z, Tang HQ, Wang N, Zhu LH. Reductive defluorination of perfluorooctanoic acid by hydrated electrons in a sulfite-mediated UV photochemical system. *J Hazard Mater.* 2013; 262(15):332–338. [PubMed: 24056245]
27. Hart EJ, Gordon S, Thomas JK. Rate Constants of Hydrated Electron Reactions with Organic Compounds<sup>1</sup>. *J Phys Chem.* 1964; 68(6):1271–1274.
28. Buxton GV, Greenstock CL, Helman WP, Ross AB. Critical review of rate constants for reactions of hydrated electrons, hydrogen atoms and hydroxyl radicals ( $\cdot\text{OH}/\cdot\text{O}^-$  in aqueous solution. *J Phys Chem Ref Data.* 1988; 17(2):513–886.
29. Gu C, Li H, Teppen BJ, Boyd SA. Octachlorodibenzodioxin formation on Fe (III)-montmorillonite clay. *Environ Sci Technol.* 2008; 42(13):4758–4763. [PubMed: 18678002]
30. Haderlein SB, Weissmahr KW, Schwarzenbach RP. Specific adsorption of nitroaromatic explosives and pesticides to clay minerals. *Environ Sci Technol.* 1996; 30(2):612–622.
31. Boyd SA, Sheng GY, Teppen BJ, Johnston CT. Mechanisms for the adsorption of substituted nitrobenzenes by smectite clays. *Environ Sci Technol.* 2001; 35(21):4227–4234. [PubMed: 11718335]
32. Liyanapattirana C, Gwaltney SR, Xia K. Transformation of triclosan by Fe (III)-saturated montmorillonite. *Environ Sci Technol.* 2010; 44(2):668–674. [PubMed: 20000674]
33. Qin C, Troya D, Shang C, Hildreth S, Helm R, Xia K. Surface catalyzed oxidative oligomerization of 17 $\beta$ -estradiol by Fe<sup>3+</sup>-saturated montmorillonite. *Environ Sci Technol.* 2015; 49(2):956–964. [PubMed: 25496116]
34. Boyd SA, Mortland MM. Dioxin radical formation and polymerization on Cu (II)-smectite. *Nature.* 1985; 316(6028):532–535.
35. Gu C, Liu C, Ding YJ, Li H, Teppen BJ, Johnston CT, Boyd SA. Clay Mediated Route to Natural Formation of Polychlorodibenzo-p-dioxins. *Environ Sci Technol.* 2011; 45(8):3445–3451. [PubMed: 21434682]
36. Gu C, Liu C, Johnston CT, Teppen BJ, Li H, Boyd SA. Pentachlorophenol radical cations generated on Fe (III)-montmorillonite initiate octachlorodibenzo-p-dioxin formation in clays: Density functional theory and fourier transform infrared studies. *Environ Sci Technol.* 2011; 45(4):1399–1406. [PubMed: 21254769]
37. Miyamoto N, Yamada Y, Koizumi S, Nakato T. Extremely stable photoinduced charge separation in a colloidal system composed of semiconducting niobate and clay nanosheets. *Angew Chem.* 2007; 46(22):4123–4127. [PubMed: 17444581]
38. Zhang J, Zhai JJ, Zhao FZ, Tao ZY. Study of soil humic substances by cross-polarization magic angle spinning <sup>13</sup>C nuclear magnetic resonance and pyrolysis-capillary gas chromatography. *Anal Chim Acta.* 1999; 378(1–3):177–182.
39. Chen H, Kenny JE. A study of pH effects on humic substances using chemometric analysis of excitation-emission matrices. *Ann Environ Sci.* 2007; 1:1–9.
40. Miura A, Fukuchi S, Okabe R, Fukushima M, Sasaki M, Sato T. Effect of different fractions of weathered pumice in the formation of humic-like substances. *Clay Miner.* 2011; 46(4):637–648.
41. Arroyo LJ, Li H, Teppen BJ, Boyd SA. A simple method for partial purification of reference clays. *Clay Clay Miner.* 2005; 53(5):511–519.
42. Becke AD. Density-functional thermochemistry. III. The role of exact exchange. *J Chem Phys.* 1993; 98(7):5648–5652.
43. Frisch, MJ., Trucks, GW., Schlegel, HB., Scuseria, GE., Robb, MA., Cheeseman, JR., Montgomery, JA., Vreven, T., Kudin, KN., Burant, JC., Millam, JM., Iyengar, SS., Tomasi, J.,

- Barone, V., Mennucci, B., Cossi, M., Scalmani, G., Rega, N., Petersson, GA., Nakatsuji, H., Hada, M., Ehara, M., Toyota, K., Fukuda, R., Hasegawa, J., Ishida, M., Nakajima, T., Honda, Y., Kitao, O., Nakai, H., Klene, M., Li, X., Knox, JE., Hratchian, HP., Cross, JB., Bakken, V., Adamo, C., Jaramillo, J., Gomperts, R., Stratmann, RE., Yazyev, O., Austin, AJ., Cammi, R., Pomelli, C., Ochterski, JW., Ayala, PY., Morokuma, K., Voth, GA., Salvador, P., Dannenberg, JJ., Zakrzewski, VG., Dapprich, S., Daniels, AD., Strain, MC., Farkas, O., Malick, DK., Rabuck, AD., Raghavachari, K., Foresman, JB., Ortiz, JV., Cui, Q., Baboul, AG., Clifford, S., Cioslowski, J., Stefanov, BB., Liu, G., Liashenko, A., Piskorz, P., Komaromi, I., Martin, RL., Fox, DJ., Keith, T., Al-Laham, MA., Peng, CY., Nanayakkara, A., Challacombe, M., Gill, PMW., Johnson, B., Chen, W., Wong, MW., Gonzalez, C., Pople, JA. Gaussian 03, revision E.01. Gaussian, Inc; Wallingford, CT: 2004.
44. McClay K, Boss C, Keresztes I, Steffan RJ. Mutations of toluene-4-monooxygenase that alter regiospecificity of indole oxidation and lead to production of novel indigoid pigments. *Appl Environ Microb*. 2005; 71(9):5476–5483.
  45. Chen QM, Yang C, Goh NK, Teo KC, Chen B. Photochemical degradation of 1,3-dinitrobenzene in aqueous solution in the presence of hydrogen peroxide. *Chemosphere*. 2004; 55(3):339–344. [PubMed: 14987932]
  46. Madden KP, Taniguchi H. In situ radiolysis time-resolved ESR studies of spin trapping by DMPO: reevaluation of hydroxyl radical and hydrated electron trapping rates and spin adduct yields. *J Phys Chem*. 1996; 100(18):7511–7516.
  47. Klots TD, Collier WB. Heteroatom derivatives of indene. Part 3. Vibrational spectra of benzoxazole, benzofuran, and indole. *Spectrochim Acta A*. 1995; 51(8):1291–1316.
  48. Walden SE, Wheeler RA. Structural and vibrational analysis of indole by density functional and hybrid Hartree-Fock/density functional methods. *J Chem Soc, Perkin Trans*. 1996; 2(12):2653–2662.
  49. Li H, Teppen BJ, Johnston CT, Boyd SA. Thermodynamics of nitroaromatic compound adsorption from water by smectite clay. *Environ Sci Technol*. 2004; 38(20):5433–5442. [PubMed: 15543748]
  50. Aggarwal V, Li H, Boyd SA, Teppen BJ. Enhanced sorption of trichloroethene by smectite clay exchanged with Cs<sup>+</sup> *Environ Sci Technol*. 2006; 40(3):894–899. [PubMed: 16509334]
  51. Charles S, Teppen BJ, Li H, Laird DA, Boyd SA. Exchangeable cation hydration properties strongly influence soil sorption of nitroaromatic compounds. *Soil Sci Soc Am J*. 2006; 70(5): 1470–1479.
  52. Van Order RB, Lindwall HG. Indole. *Chem Rev*. 1942; 30(1):69–96.
  53. Yokoyama MT, Carlson JR. Microbial metabolites of tryptophan in the intestinal tract with special reference to skatole. *Am J Clin Nutr*. 1979; 32(1):173–178. [PubMed: 367144]
  54. Hawe SM, Walker N, Moss BW. The effects of dietary fibre, lactose and antibiotic on the levels of skatole and indole in faeces and subcutaneous fat in growing pigs. *Anim Prod*. 1992; 54(3):413–419.
  55. Jensen MT, Cox RP, Jensen BB. 3-Methylindole (skatole) and indole production by mixed populations of pig fecal bacteria. *Appl Environ Microb*. 1995; 61(8):3180–3184.
  56. Martino PD, Fursy R, Bret L, Sundararaju B, Phillips RS. Indole can act as an extracellular signal to regulate biofilm formation of *Escherichia coli* and other indole-producing bacteria. *Can J Microbiol*. 2003; 49(7):443–449. [PubMed: 14569285]
  57. Lee DS, Jeon CO, Park JM, Chang KS. Hybrid neural network modeling of a full scale industrial wastewater treatment process. *Biotechnol Bioeng*. 2002; 78(6):670–682. [PubMed: 11992532]
  58. Li YM, Gu GW, Zhao JF, Yu HQ, Qiu YL, Peng YZ. Treatment of coke-plant wastewater by biofilm systems for removal of organic compounds and nitrogen. *Chemosphere*. 2003; 52(6):997–1005. [PubMed: 12781233]

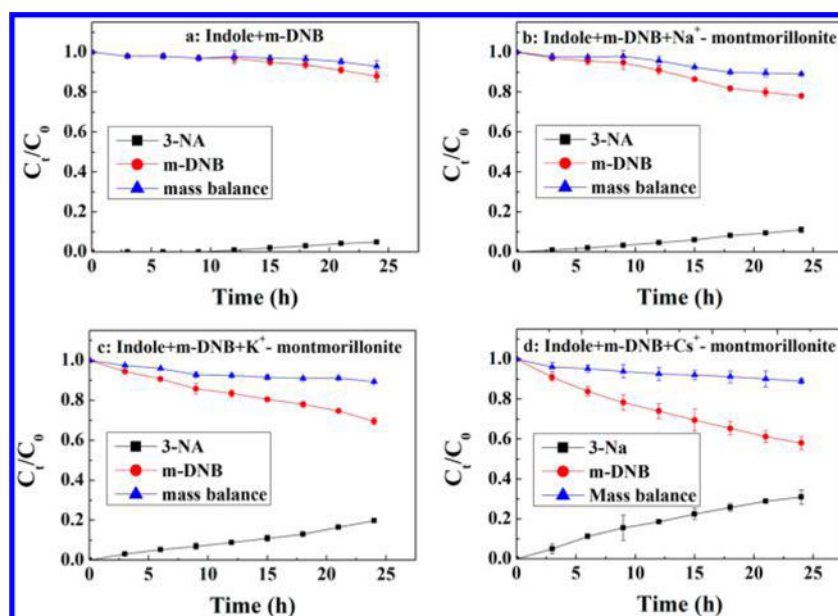


**Figure 1.**

Photoreduction of m-DNB by indole under simulated solar light irradiation as a function of time with (a) no montmorillonite (control experiment) and in the presence of (b) Na<sup>+</sup>-montmorillonite, (c) K<sup>+</sup>-montmorillonite, and (d) Cs<sup>+</sup>-montmorillonite. Experimental conditions: the initial concentrations of m-dinitrobenzene, indole, and clay mineral were 0.0125 mM, 0.5 mM, and 1 g L<sup>-1</sup>, respectively. pH was controlled at 7.3 with 5 mM phosphate buffer; a 500W xenon lamp was used to simulate solar light irradiation. Error bars are the standard deviations of triplicate analyses.

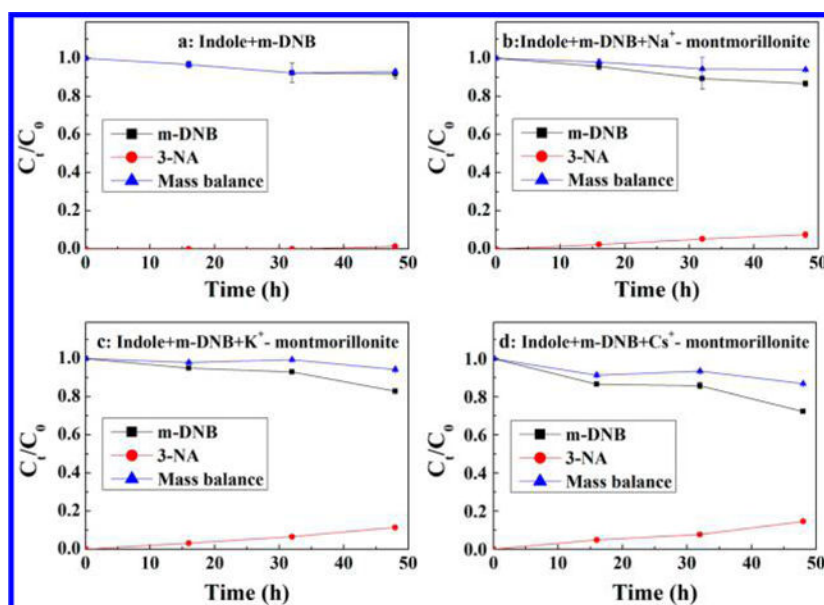


**Figure 2.**

Photoreduction of m-DNB by indole under sunlight irradiation as a function of time with (a) no montmorillonite (control experiment), and in the presence of (b) Na<sup>+</sup>-montmorillonite, (c) K<sup>+</sup>-montmorillonite, and (d) Cs<sup>+</sup>-montmorillonite. Experimental conditions: the initial concentrations of m-dinitrobenzene, indole, and clay mineral were 0.0125 mM, 0.5 mM, and 1 g L<sup>-1</sup>, respectively; pH was controlled at 7.3 with 5 mM phosphate buffer. Sunlight exposure was performed from 9 a.m. to 5 p.m. on sunny or partly cloudy days from March 22 to 27, 2014. Error bars are the standard deviations of triplicate analyses.

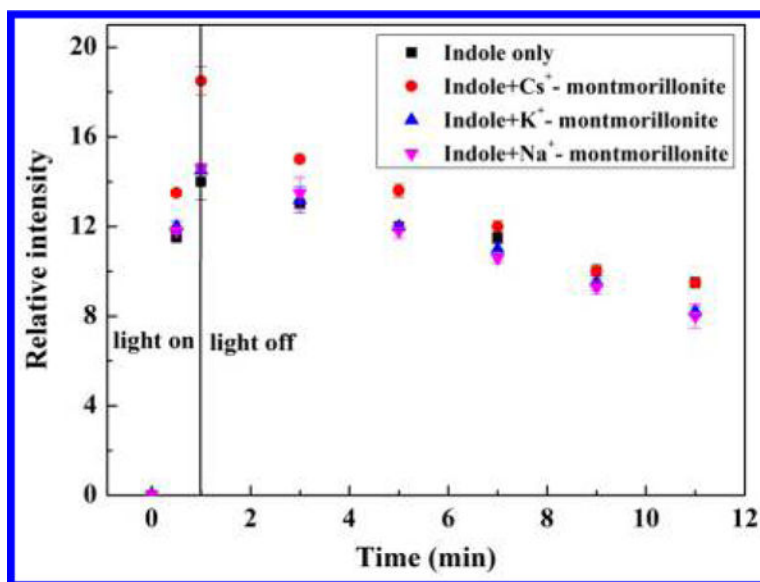


**Figure 3.**

Kinetics of buildup and decay of DMPO-H adduct as a function of the irradiation time in the presence of indole and Na<sup>+</sup>, K<sup>+</sup>, or Cs<sup>+</sup>-montmorillonite. Experimental conditions: the initial concentrations of DMPO, indole, and clay mineral were 10 mM, 0.5 mM, and 1 g L<sup>-1</sup>, respectively. Error bars are the standard deviations of triplicate analyses. Linear kinetic plot of the spectral intensities of the DMPO-H illustrated the rapid production of hydrated electrons during light irradiation.

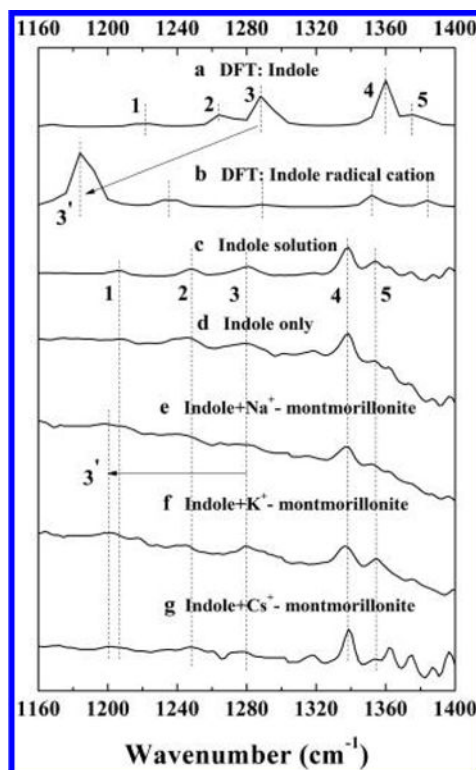


**Figure 4.**

Comparison of calculated and experimental IR spectra: calculated IR spectra of (a) indole and (b) indole radical cation; observed IR spectra of (c) indole in solution, (d) indole solution irradiated by simulated solar light, and indole solution irradiated by simulated solar light in the presence of (e) Na<sup>+</sup>-montmorillonite, (f) K<sup>+</sup>-montmorillonite, and (g) Cs<sup>+</sup>-montmorillonite. Experimental conditions: the initial concentrations of indole and clay mineral were 10 mM and 10 g L<sup>-1</sup>, respectively; pH was controlled at 7.3 with 5 mM phosphate buffer.

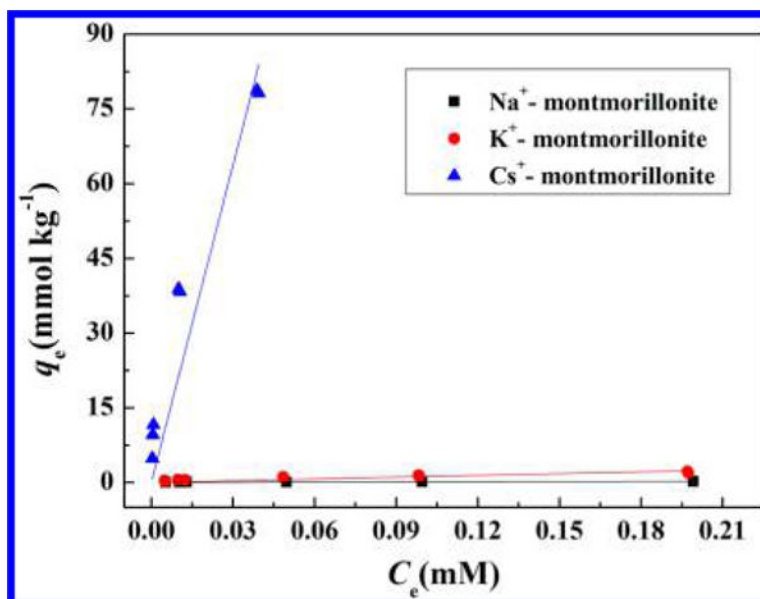


**Figure 5.**

Adsorption isotherms of m-DNB on Na<sup>+</sup>-, K<sup>+</sup>- and Cs<sup>+</sup>-montmorillonite.  $q_e$  is the amount of m-DNB adsorbed on montmorillonite clay mineral (mmol kg<sup>-1</sup>), and  $C_e$  is the equilibrium concentration of m-DNB (mM). Experimental conditions: 10 mg montmorillonite, m-DNB with initial concentrations ranging from 0.005 to 0.2 mM, reaction medium 10 mL phosphate buffer (5 mM, pH = 7.3).

**Table 1**

Fitted Linear Adsorption Coefficients for m-DNB, Indole, 3-NA, and NB Adsorption on Na<sup>+</sup>, K<sup>+</sup>, and Cs<sup>+</sup>-Montmorillonite<sup>a</sup>

smectite clay	m-DNB		indole		3-NA		NB	
	$K_d$ (L kg <sup>-1</sup> )	$R^2$	$K_d$ (L kg <sup>-1</sup> )	$R^2$	$K_d$ (L kg <sup>-1</sup> )	$R^2$	$K_d$ (L kg <sup>-1</sup> )	$R^2$
Na <sup>+</sup> -montmorillonite	1.23	0.828	3.92	0.995	0.39	0.810	0.55	0.916
K <sup>+</sup> -montmorillonite	11.82	0.894	3.88	0.989	0.34	0.811		
Cs <sup>+</sup> -montmorillonite	2121.12	0.931	5.13	0.980	18.68	0.987		
kaolinite	1.18	0.909	1.66	0.957				
silica	0.91	0.957	1.76	0.921				

<sup>a</sup>The adsorption data were fitted with a linear isotherm model:  $q_e = K_d C_e$ , where  $q_e$  is the amount of adsorbate adsorbed on mineral surfaces (mmol kg<sup>-1</sup>),  $K_d$  is the linear adsorption coefficient (L kg<sup>-1</sup>),  $C_e$  is the equilibrium concentration (mM), and  $R^2$  is the coefficient of determination from the overall regression analysis.